Proceedings of the 2016 IEEE
International Conference on Robotics and Biomimetics
Qingdao, China, December 3-7, 2016

Kinematics Analysis of a 4-DOF Underwater Manipulator Installed on the Vehicle

Yu Wang, Shuo Wang, Chao Zhou*, and Min Tan

***Abstract*— The paper addresses kinematics analysis of a 4-DOF underwater manipulator, which can be installed on an Underwater Vehicle-Manipulator System (UVMS). First, the kinematic model of the manipulator is built. Next, the computation for the centers of weight and buoyancy is provided for the analysis of the coupling between the vehicle and the manipulator. Then the calibration including camera calibration and hand-eye calibration for its free-floating manipulation is introduced. Finally, experimental results of autonomous manipulation are given to deduce the kinematics characteristic of the underwater manipulator.**

I. Introduction

An Underwater Vehicle-Manipulator System (UVMS) is served as an important tool for ocean resource exploitation, underwater equipment maintenance, underwater salvage. Autonomous manipulation of the UVMS is very challenging. Because it is a nonlinear, highly coupled system. So autonomous control of the UVMS has drawn more and more attention. Mohan et al. employed a disturbance observer to achieve the motion control between the vehicle and the manipulator for underwater manipulation [1]. Moreover, Han et al. proposed an adaptive control framework merging optimal PID control with restoring vector adaptation for tracking control of the UVMS [2]. And Esfahani et al. presented a Time Delay Control (TDC) method including a time-delay-estimation term, a Terminal Sliding Mode (TSM) term and a PID term to implement trajectory tracking of the UVMS [3]. Farivarnejad et al. designed Multiple Impedance Control (MIC) to realize target grasping of a dual arm underwater vehicle-manipulator system [4]. Olguin-Diaz et al. applied a passivity-based force-motion control scheme for tracking control of the UVMS [5].

Recently, two projects are devoted to autonomous manipulation of the UVMS, which are the SAUVIM project and the TRIDENT project. In the SAUVIM project, autonomous manipulation of the UVMS was achieved [6], [7]. In the TRIDENT project, floating underwater manipulation of an AUV equipped with a lightweight manipulator was implemented [8]–[11].

This work was supported in part by the National Natural Science Foundation of China under Grant 51175496, 61233014, 61333016, in part by the National Key Technology Support Program 2015BAF01B01, in part by the Foundation for Innovative Research Groups of the National Natural Science Foundation of China under Grant 61421004, and in part by the Beijing Natural Science Foundation under Grant 4152054.

Y. Wang, S. Wang, C. Zhou, and M. Tan are with the State Key Laboratory of Management and Control for Complex Systems, Institute of Automation, Chinese Academy of Sciences, Beijing 100190, China.
(e-mail: chao.zhou@ia.ac.cn)

However, high-speed arm motions would result in the coupling between the manipulator and the vehicle [8]. Therefore, we have designed and developed a 4-DOF underwater manipulator with a lightweight multi-link structure, which could reduce the coupling between the vehicle and the manipulator. Moreover, its free-floating autonomous operation was realized [12]. The main aim of this paper is to analyze the kinematics characteristic of this underwater manipulator. The rest of the paper is arranged as follows. Based on D–H parameters model, the kinematics of underwater manipulator is built in Section II. The computation for the centers of weight and buoyancy for the analysis of the coupling between the vehicle and the manipulator is given in Section III. Since the vision-based control system is employed, calibration which consists of camera calibration and hand-eye calibration for autonomous manipulation is introduced Section IV. Experiments are given in Section V. Finally, conclusion and future work are summarized in Section VI.

II. Kinematics of the Underwater Manipulator

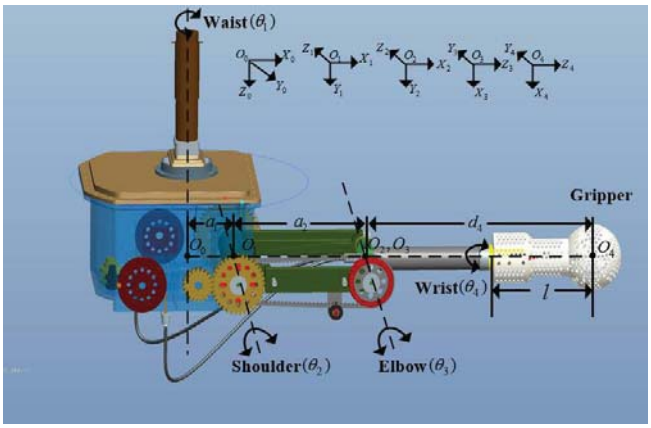

Fig. 1. Denavit–Hartenberg (D–H) reference frames.

The novel manipulator with a multi-link structure is shown in Fig. 1, whose detailed mechanical design has been presented and introduced in [12]. We define the initial position of the manipulator(See Fig. 1): Gripper is closed. Link 1 and Link 2 are both parallel to the coronal plane of the manipulator. Furthermore, the plane formed by the open Gripper is also parallel to this coronal plane. In Fig. 1, the Denavit–Hartenberg (D-H) reference frames including $O_0X_0Y_0Z_0 \sim O_5X_5Y_5Z_5$ are assigned. Based on the D-H parameters model, the kinematics of the underwater manipulator is easy to be

established. The link transformation matrixes are as follows:

$$A_1 = \begin{bmatrix} \cos\theta_1 & 0 & \sin\theta_1 & a_1\cos\theta_1 \\ \sin\theta_1 & 0 & -\cos\theta_1 & a_1\sin\theta_1 \\ 0 & 1 & 0 & 0 \\ 0 & 0 & 0 & 1 \end{bmatrix} \quad (1)$$

$$A_2 = \begin{bmatrix} \cos\theta_2 & -\sin\theta_2 & 0 & a_2\cos\theta_2 \\ \sin\theta_2 & \cos\theta_2 & 0 & a_2\sin\theta_2 \\ 0 & 0 & 1 & 0 \\ 0 & 0 & 0 & 1 \end{bmatrix} \quad (2)$$

$$A_3 = \begin{bmatrix} -\sin\theta_3 & 0 & \cos\theta_3 & 0 \\ \cos\theta_3 & 0 & \sin\theta_3 & 0 \\ 0 & 1 & 0 & 0 \\ 0 & 0 & 0 & 1 \end{bmatrix} \quad (3)$$

$$A_4 = \begin{bmatrix} \cos\theta_4 & -\sin\theta_4 & 0 & 0 \\ \sin\theta_4 & \cos\theta_4 & 0 & 0 \\ 0 & 0 & 1 & d_4 \\ 0 & 0 & 0 & 1 \end{bmatrix} \quad (4)$$

where A_1, A_2, A_4 and A_3 are the transformation matrixes of the link frames; $\theta_i (i = 1,2,3,4)$ represent the joint angles of Waist, Shoulder, Elbow, and Wrist, respectively. θ_5 is defined as the opening angle of Gripper. a_1 is the link length between Waist and Shoulder; a_2 is the link length between Shoulder and Elbow; d_4 is the offsets of Wrist. The specific parameters are listed in Table I. Hence, the pose of the end effector

TABLE I
D–H PARAMETERS

Link	$\theta(^\circ)$	d(mm)	a(mm)	$\alpha(^\circ)$
1	θ_1	0	67	90
2	θ_2	0	189.95	0
3	θ_3+90	0	0	90
4	θ_4	323	0	0

expressed in the reference frame $O_0X_0Y_0Z_0$ is obtained by

$$^0T_E = A_1A_2A_3A_4 \quad (5)$$

III. THE COMPUTATION FOR THE CENTERS OF WEIGHT AND BUOYANCY

The changing curves of centers of gravity and buoyancy during the grasping process of the arm are usually required, which can help to analyze the coupling between the vehicle and the manipulator. Next, we give the computation for the centers of weight and buoyancy of the manipulator and UVMS in the reference frame $O_0X_0Y_0Z_0$(See Fig. 1).

The center of weight and the center of buoyancy of the vehicle are respectively denoted by $P_{gv}(x_{gv}, y_{gv}, z_{gv})$ and $P_{bv}(x_{bv}, y_{bv}, z_{bv})$ in the $O_0X_0Y_0Z_0$ frame. Analogously, the center of weight and the center of buoyancy of the ith component of the underwater arm in the $O_jX_jY_jZ_j (j = 1...5)$ frame are denoted by $P_{g,i,j}(x_{g,i,j}, y_{g,i,j}, z_{g,i,j})$ and $P_{b,i,j}(x_{b,i,j}, y_{b,i,j}, z_{b,i,j})$, respectively. Table II shows the main components' weight and the relationship between the component of the underwater arm and the i value. Thus when $i = 1,2\ or\ 3$, $P_{g,i,0}$ and $P_{b,i,0}$ can be calculated as

TABLE II
MAIN COMPONENTS' WEIGHT AND THE RELATIONSHIP BETWEEN THE COMPONENT AND THE i VALUE

Components	i	Weight in air(kg)	Weight in water(kg)
Base	1	11.04	4.39
Link 1	2	0.44	0.159
Link 2	3	0.311	0.106
Gripper	4	0.138	0.043

$$\begin{bmatrix} P^T_{l,i,0} \\ 0 \end{bmatrix} = T_i \cdot \begin{bmatrix} \cos\theta_i & -\sin\theta_i & 0 & 0 \\ \sin\theta_i & \cos\theta_i & 0 & 0 \\ 0 & 0 & 1 & 0 \\ 0 & 0 & 0 & 1 \end{bmatrix} \begin{bmatrix} P^T_{l,i,(i-1)} \\ 0 \end{bmatrix} \quad (6)$$

where, l denotes g or b, $P_{l,i,(i-1)}$ is a known value which can be obtained by Pro/Engineer software, T_i can be determined by

$$T_i = \begin{cases} 1 & i = 1 \\ A_1 \ldots A_{i-1} & i = 2,3 \end{cases} \quad (7)$$

As the gripper is evenly distributed, $P^T_{i,4,5}$ can be given by

$$P_{i,4,5} = (0, 0, (z_0 + l)\cos\frac{\theta_5}{2} - l) \quad (8)$$

where z_0 is the initial Z value of the gripper in the reference frame $O_5X_5Y_5Z_5$ when the gripper is closed, l (marked in Fig. 1) is the distance between initial position of the gripper and O_5. So for the case of $i = 4$, we can get

$$\begin{bmatrix} P^T_{l,4,0} \\ 0 \end{bmatrix} = A_1A_2A_3A_4 \begin{bmatrix} P^T_{l,4,5} \\ 0 \end{bmatrix} \quad (9)$$

Consequently, the center of weight (denoted by $P_{gm}(x_{gm}, y_{gm}, z_{gm})$) and the center of buoyancy (denoted by $P_{bm}(x_{bm}, y_{bm}, z_{bm})$) of the manipulator are

$$P_{gm} = \frac{1}{G_m} \cdot \begin{bmatrix} G_1 & G_2 & G_3 & G_4 \end{bmatrix} \begin{bmatrix} P_{g,1,0} \\ P_{g,2,0} \\ P_{g,3,0} \\ P_{g,4,0} \end{bmatrix} \quad (10)$$

$$P_{bm} = \frac{1}{B_m} \cdot \begin{bmatrix} B_1 & B_2 & B_3 & B_4 \end{bmatrix} \begin{bmatrix} P_{b,1,0} \\ P_{b,2,0} \\ P_{b,3,0} \\ P_{b,4,0} \end{bmatrix} \quad (11)$$

where, G_i is the gravity of the ith component of the underwater manipulator, B_i is the buoyancy of the ith component of the underwater manipulator, G_m and B_m are the total gravity and buoyancy of the underwater manipulator, respectively. Hence, the positions of UVMS's centers of gravity and

buoyancy (denoted by $P_{gu}(x_{gu}, y_{gu}, z_{gu})$ and $P_{bu}(x_{bu}, y_{bu}, z_{bu})$ respectively) are calculated as

$$P_{gu} = \frac{1}{G_m + G_v} \begin{bmatrix} G_m & G_v \end{bmatrix} \begin{bmatrix} P_{gm} \\ P_{gv} \end{bmatrix} \tag{12}$$

$$P_{bu} = \frac{1}{B_m + B_v} \begin{bmatrix} B_m & B_v \end{bmatrix} \begin{bmatrix} P_{bm} \\ P_{bv} \end{bmatrix} \tag{13}$$

where, G_v, B_v are the gravity and buoyancy of the vehicle, respectively.

Thus the changing curves of centers of gravity and buoyancy during the grasping process of the arm can be obtained.

IV. CALIBRATION

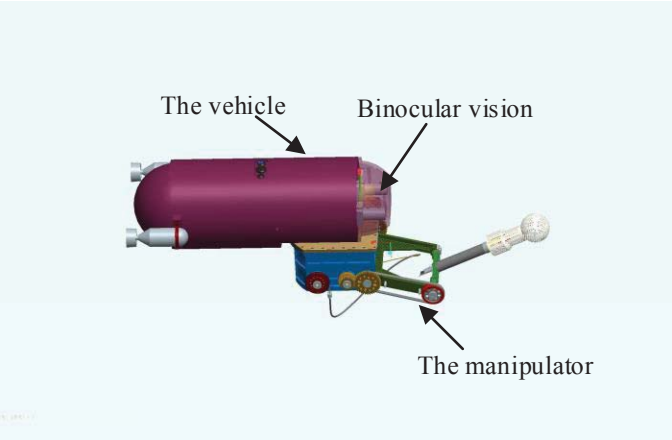

Fig. 2. Concept design of UVMS

In order to deduce the characteristic of the underwater manipulator, the manipulator is installed on a vehicle as illustrated in Fig. 2. The vehicle weight in air is $27kg$, and the underwater vehicle-manipulator system (UVMS) could just be suspended in water. Two cameras are installed in front of the vehicle. The vision-based control system of the manipulator is used for the manipulation, which has been introduced in detail in our previous work [12]. Here we only give the calibration for the two cameras and hand-eye.

A. Camera calibration

The parameters of the camera include intrinsic parameters and external parameters. Here the external parameters of the camera include three-dimensional translation and the rotation matrix of the camera relative to the body-fixed frame.

These parameters can be expressed as

The intrinsic parameter matrix:

$$M_{in} = \begin{pmatrix} k_x & k_s & u_0 \\ 0 & k_y & v_0 \\ 0 & 0 & 1 \end{pmatrix} \tag{14}$$

The extrinsic parameter matrix:

$$M_{ex} = \begin{pmatrix} R & p \\ 0 & 1 \end{pmatrix}, R = \begin{pmatrix} r_1 & r_2 & r_3 \\ r_4 & r_5 & r_6 \\ r_7 & r_8 & r_9 \end{pmatrix}, p = \begin{pmatrix} p_x \\ p_y \\ p_z \end{pmatrix} \tag{15}$$

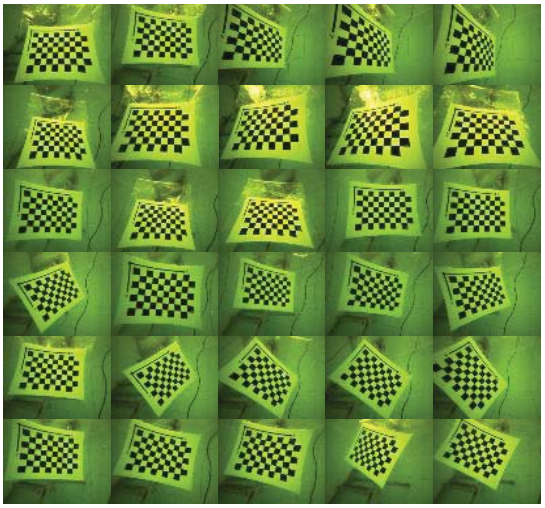

(a) Pictures captured by the left camera

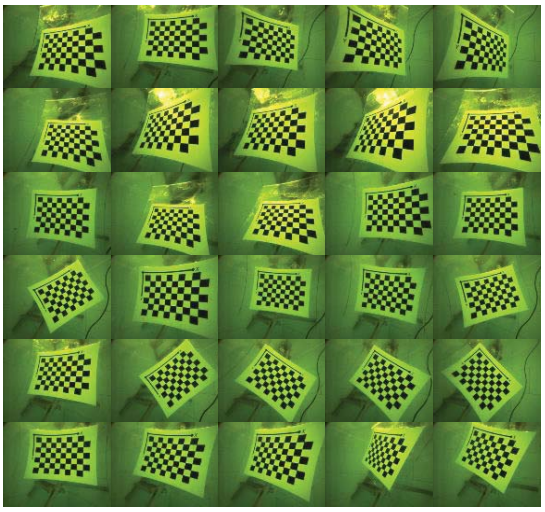

(b) Pictures captured by the left camera

Fig. 3. Pictures captured by the two cameras

The method of calibration is mature, so it is not introduced in this paper. The captured pictures are seen in Fig. 3. We use Matlab Calibration Toolbox to realize camera calibration. Fig. 4 depicts the relative relationships between the two cameras and calibration board.

Next, the results are directly listed by calibration.

The intrinsic parameter matrix of the left camera:

$$M_{in-left} = \begin{pmatrix} 209.1199 & 0.7944 & 192.1148 \\ 0 & 198.0329 & 127.5282 \\ 0 & 0 & 1 \end{pmatrix} \tag{16}$$

The tangential distortion parameters of left camera: [0.0018 0.1097].

The radial distortion parameters of left camera: [0.4199 0.1892 0.1325].

The intrinsic parameter matrix of the right camera:

$$M_{in-right} = \begin{pmatrix} 209.8340 & 0.075 & 135.8079 \\ 0 & 199.3363 & 121.3709 \\ 0 & 0 & 1 \end{pmatrix} \tag{17}$$

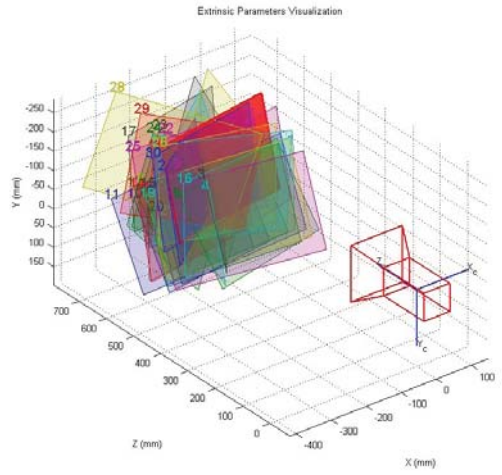

(a) The relative relationship between the left camera and calibration board

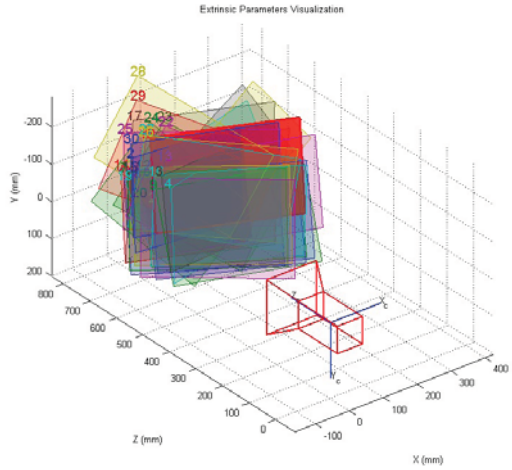

(b) The relative relationship between the right camera and calibration board

Fig. 4. The relative relationships between the two cameras and calibration board

The tangential distortion parameters of right camera: [-0.0007 -0.1098].

The radial distortion parameters of right camera: [0.3953 -0.0797 0.0173].

The reference frame marked on the board in the final one of Fig. 3 is selected as the body-fixed frame. The extrinsic parameter matrix of the left camera relative to the body-fixed frame is given as

$$M_{ex-left} = \begin{pmatrix} 0.9604 & -0.0160 & -0.2780 & -321.7106 \\ 0.0729 & 0.9780 & 0.1956 & -206.1425 \\ 0.2688 & -0.2081 & 0.9404 & 557.0300 \\ 0 & 0 & 0 & 1 \end{pmatrix} \tag{18}$$

The extrinsic parameter matrix of the right camera relative to the body-fixed frame is given as

$$M_{ex-right} = \begin{pmatrix} 0.9529 & -0.1045 & 0.2848 & -63.2549 \\ 0.0472 & 0.9784 & 0.2013 & -196.9730 \\ -0.2997 & -0.1783 & 0.9372 & 672.8579 \\ 0 & 0 & 0 & 1 \end{pmatrix} \tag{19}$$

B. Hand-eye calibration

Fig. 5. Hand-eye calibration.

As illustrated in Fig. 5, the red target is placed inside the gripper. So the position of target center expressed in the $O_0X_0Y_0Z_0$ frame (denoted as P_B) is known. Meanwhile, the position of target center expressed in the body-fixed frame (denoted as P_A) can be calculated by 3-D reconstruction method [13]. The relationship between P_B and P_A is given as

$$P_B = R \cdot P_A + T. \tag{20}$$

Several sets of data including the position expressed in two different frame can be obtained by changing the position of the gripper. Thus the method presented in [14] can be applied to get the extrinsic parameter matrix between the body-fixed frame and the reference frame $O_0X_0Y_0Z_0$.

The hand-eye calibration results are given as

$$R = \begin{bmatrix} 0.0456 & 0.0745 & 0.9935 \\ -0.9963 & 0.0016 & 0.0456 \\ 0.0018 & -0.9946 & 0.0745 \end{bmatrix} \tag{21}$$

$$T = \begin{bmatrix} 545.519 \\ 55.444 \\ -105.002 \end{bmatrix} \tag{22}$$

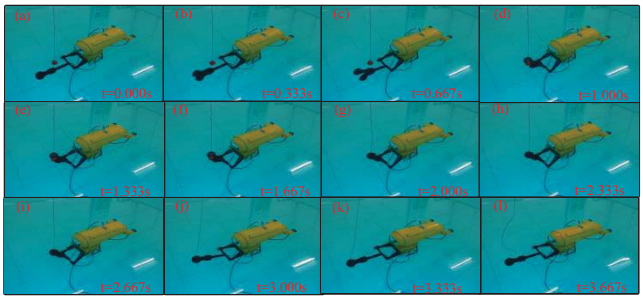

Fig. 6. Consecutive snapshots of autonomous manipulation.

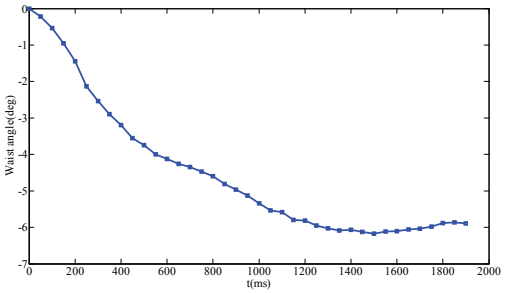

(a)

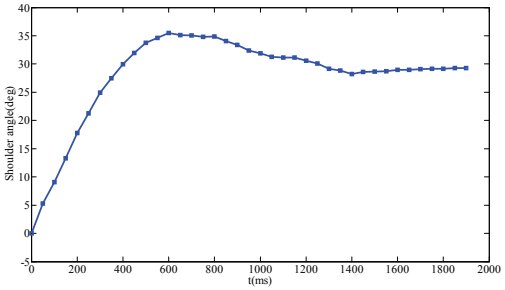

(b)

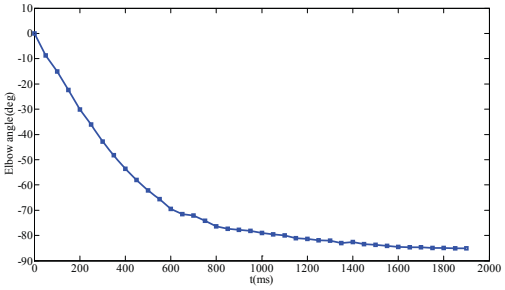

(c)

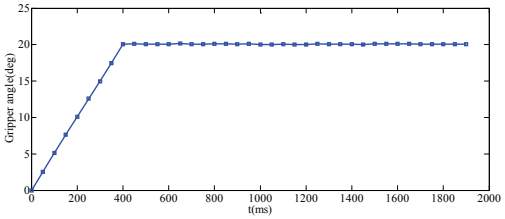

(d)

Fig. 7. Time history of joint angles. (a) Time history of Waist angle. (b) Time history of Shoulder angle. (c) Time history of Elbow angle. (d) Time history of Gripper's opening angle.

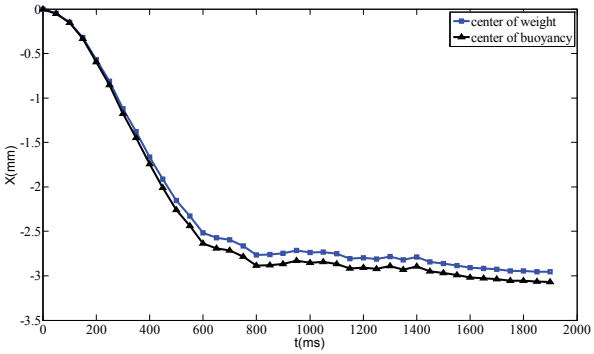

(a)

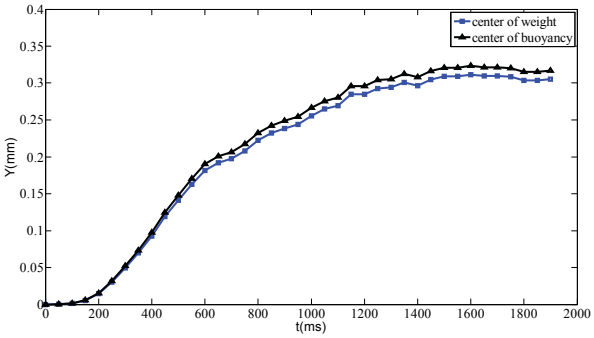

(b)

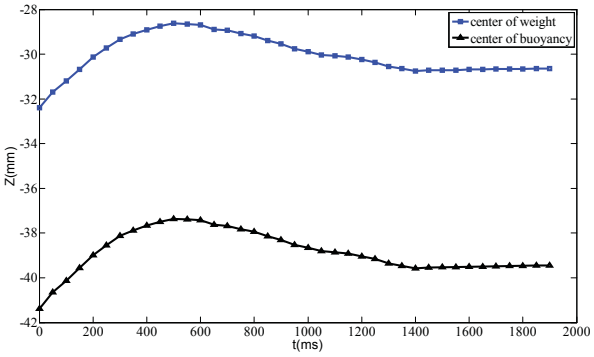

(c)

Fig. 8. Time history of positions of the centers of the manipulator's weight and buoyancy in the $O_0X_0Y_0Z_0$ frame by estimation. (a) Time history of X values of the centers of the manipulator's weight and buoyancy. (b) Time history of Y values of the centers of the manipulator's weight and buoyancy. (c) Time history of Z values of the centers of the manipulator's weight and buoyancy.

V. EXPERIMENT OF MANIPULATION

Experiment of manipulation is conducted in a swimming pool. A target is put in the vision system, and free-floating autonomous manipulation is achieved. Fig. 6 shows consecutive snapshots of free-floating autonomous manipulation, where Fig. 6 (a)–(f) show the process of approaching the target, Fig. 6 (g)–(l) show the process of closing the gripper and returning to the initial position. Time history of joint angles of the underwater manipulator is depicted in Fig. 7. From Fig. 7, we can know that the relative high-speed arm movement is realized.

Furthermore, Fig. 8 and Fig. 9 give the changes in the

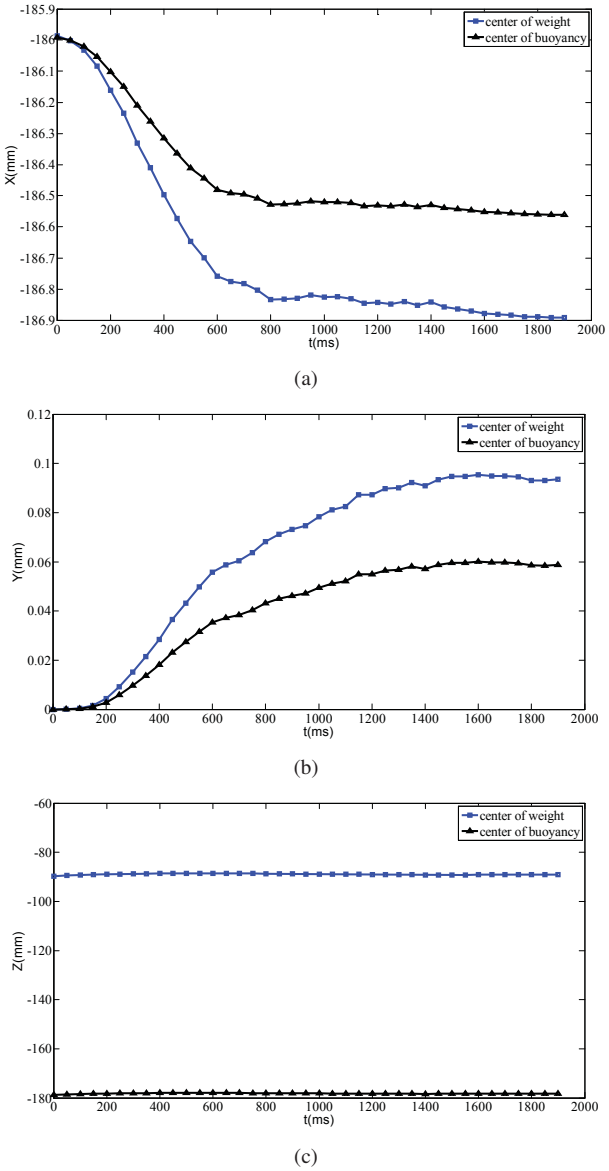

Fig. 9. Time history of positions of the centers of the UVMS's weight and buoyancy in the $O_0X_0Y_0Z_0$ frame by estimation. (a) Time history of X values of the centers of the UVMS's weight and buoyancy. (b) Time history of Y values of the centers of the UVMS's weight and buoyancy. (c) Time history of Z values of the centers of the UVMS's weight and buoyancy.

positions of mass center and buoyancy center of the underwater manipulator and UVMS in the $O_0X_0Y_0Z_0$ frame respectively, which are calculated according to Section III. From these two figures, we can see that the small changes of the centers of weight and buoyancy occur during arm maneuvers, and the changes are less than $5mm$. Moreover, the change rules in the positions of the centers of weight and buoyancy are substantially similar. In the experiment of manipulation, high-speed arm movement can be achieved, which illustrates that the coupling between the vehicle and the manipulator caused by the changes in the positions of centers of mass and buoyancy is reduced effectively.

VI. Conclusion and Future Work

A 4-DOF underwater manipulator has been developed [12]. In this paper, kinematics analysis of this underwater manipulator is presented. The kinematic model of the manipulator is established. In order to deduce the coupling between the vehicle and the manipulator, the computation for the centers of weight and buoyancy is given. Moreover, the calibration for its free-floating manipulation is introduced. Experimental results of autonomous manipulation are provided to deduce the kinematics characteristic of the underwater manipulator.

Future research will concentrate on two aspects: first, an Underwater Bio-inspired Vehicle-Manipulator System (UBVMS) will be developed based on our previous work [12], and its autonomous operation will be studied; second, vehicle-arm coordination control of the UBVMS will be investigated.

References

[1] S. Mohan, and J. Kim, "Coordinated motion control in task space of an autonomous underwater vehicleCmanipulator system," *Ocean. Eng.*, vol. 104, pp. 155–167, 2015.

[2] J. Han, and W. K. Chung, "Active use of restoring moments for motion control of an underwater vehicle-manipulator system," *IEEE J. Ocean. Eng.*, vol. 39, no. 1, pp. 100–109, 2014.

[3] H. N. Esfahani, V. Azimirad, and M. Danesh, "A Time Delay Controller included terminal sliding mode and fuzzy gain tuning for Underwater Vehicle-Manipulator Systems," *Ocean. Eng.*, vol. 107, pp. 97–107, 2015.

[4] H. Farivarnejad, and S. A. A. Moosavian, "Multiple Impedance Control for object manipulation by a dual arm underwater vehicleCmanipulator system," *Ocean. Eng.*, vol. 89, pp. 82–98, 2014.

[5] E. Olguin-Diaz, G. Arechavaleta, G. Jarquin, and V. Parra-Vega, "A passivity-based model-free force-motion control of underwater vehicle-manipulator systems," *IEEE Trans. Robot.*, vol. 29, no. 6, pp. 1469–1484, 2013.

[6] G. Marani, S. K. Choi, and J. Yuh, "Underwater autonomous manipulation for intervention missions AUVs," *Ocean. Eng.*, vol. 36, no. 1, pp. 15–23, 2009.

[7] C. A. Simpkins, "Introduction to autonomous manipulation: Case study with an underwater robot, SAUVIM" *IEEE Rob. Autom. Mag.*, vol. 4, no. 21, pp. 109–110, 2014.

[8] J. J. Fernandez, M. Prats, P. J. Sanz, J. C. Garcia, R. Marin, M. Robinson, D. Ribas, and P. Ridao, "Grasping for the seabed: developing a new underwater robot arm for shallow-water intervention," *IEEE Rob. Autom. Mag.*, vol. 20, no. 4, pp. 121–130, 2013.

[9] J. R. Bemfica, C. Melchiorri, L. Moriello, G. Palli, and U. Scarcia, "A three-fingered cable-driven gripper for underwater applications," in *Proc. IEEE Int. Conf. Robot. Autom.*, Hong Kong, China, 2014, pp. 2469–2474.

[10] D. Ribas, P. Ridao, A. Turetta, C. Melchiorri, G. Palli, J. J. Fernandez, and P. J. Sanz, "I-AUV mechatronics integration for the TRIDENT FP7 project," *IEEE/ASME Trans. on Mechatronics*, vol. 20, no. 5, pp. 2583–2592, 2015.

[11] E. Simetti, G. Casalino, S. Torelli, A. Sperind, and A. Turetta, "Underwater floating manipulation for robotic interventions," in *Proc. 19th IFAC World Congress*, Cape Town, South Africa, 2014, pp. 3358–3363.

[12] Y. Wang, S. Wang, Q. Wei, M. Tan, C. Zhou, and J. Yu, "Development of an underwater manipulator and its free-floating autonomous operation," *IEEE/ASME Trans. on Mechatronics*, vol. 21, no. 2, pp. 815–824, 2016.

[13] H. Li, Y. L. Chen, T. Chang, X. Wu, Y. Ou, and Y. Xu, "Binocular vision positioning for robot grasping," in *Proc. IEEE Int. Conf. Robot. Biomimetics*, Phuket, Thailand, 2011, pp. 1522–1527.

[14] B. K. P. Horn, "Closed-form solution of absolute orientation using unit quaternions," *J. Opt. Soc. Amer. A*, vol. 4, no. 4, pp. 629–642, 1987.